Strong momentum-dependent electron–magnon renormalization of a surface resonance on iron

Cite as: Appl. Phys. Lett. **120**, 202404 (2022); https://doi.org/10.1063/5.0089688
Submitted: 28 February 2022 • Accepted: 03 May 2022 • Published Online: 17 May 2022

Beatrice Andres, **Martin Weinelt,** **Hubert Ebert, et al.**

Applied Physics Letters ARTICLE scitation.org/journal/apl

Strong momentum-dependent electron–magnon renormalization of a surface resonance on iron

Cite as: Appl. Phys. Lett. **120**, 202404 (2022); doi: 10.1063/5.0089688
Submitted: 28 February 2022 · Accepted: 3 May 2022 ·
Published Online: 17 May 2022

Beatrice Andres,[1] Martin Weinelt,[1,a)] Hubert Ebert,[2] Jürgen Braun,[2] Alex Aperis,[3] and Peter M. Oppeneer[3]

AFFILIATIONS

[1]Fachbereich Physik, Freie Universität Berlin, Arnimallee 14, 14195 Berlin, Germany
[2]Ludwig-Maximilians-Universität München, Butenandtstr. 5-13, 81377 München, Germany
[3]Department of Physics and Astronomy, Uppsala University, P. O. Box 516, 75120 Uppsala, Sweden

Note: This paper is part of the APL Special Collection on Ultrafast and Terahertz Spintronics.
[a)]**Author to whom correspondence should be addressed:** weinelt@physik.fu-berlin.de

ABSTRACT

The coupling of electrons to spin excitations and the generation of magnons is essential for spin mixing in the ultrafast magnetization dynamics of 3*d* ferromagnets. Although magnon energies are generally much larger than phonon energies, until now their electronic band renormalization effect in 3*d* ferromagnets suggests a significantly weaker quasiparticle interaction. Using spin- and angle-resolved photoemission, we show an extraordinarily strong renormalization leading to two-branch splitting of an iron surface resonance at ∼200 meV. Its strong magnetic linear dichroism unveils the magnetic nature and momentum dependence of the energy renormalization. By determining the frequency- and momentum-dependent self-energy due to generic electron–boson interaction to compute the resultant electron spectral function, we suggest that the surface-state splitting can be described by strong coupling to an optical spin wave in an iron thin film.

The coupling between electrons and magnons is a fundamental quasiparticle interaction, which affects numerous ordering processes in magnetic materials. In spintronics, it plays an important role for spin-polarized tunneling[1] and recent works give the first evidence that magnons can drive ultrafast magnetization dynamics within 100 fs.[2–7] In contrast, electron–phonon equilibration requires typically 1–2 ps. This implies that the optically excited electrons couple to the spin system while the lattice is still cold. Nevertheless, so far only few works could capture the influence of such electron–magnon quasiparticle coupling in ferromagnetic metals.[8–12]

In photoelectron spectroscopy, electron–boson coupling often manifests as kinks in the electronic band structure. The interaction of metal electrons with elementary excitations leads to a renormalization of their energy, described by the self-energy $\Sigma(\boldsymbol{k},\omega)$ entering the spectral function.[13] The band dispersion $E(\boldsymbol{k}) - \Re\mathfrak{e}\Sigma(\boldsymbol{k},\omega)$ will differ from that expected for the non-interacting case $E(\boldsymbol{k})$. The electrons become dressed by excitations. They form quasiparticles with increased mass and show consequently a reduced slope of the band dispersion. Outside the characteristic energy scale ω of the coupled excitations, the electrons resume the non-coupling, steeper band dispersion, leading to kinks in the overall band dispersion. This quasiparticle renormalization is equally induced by interactions with phonons,[14–16] electrons,[17–20] magnons,[8,9] and plasmons.[21] Apart from kinks in the electronic bands, strong electron–boson coupling can also be reflected in replica band or satellite formation, which was, for example, detected for hydrogen-induced surface states on W(110),[14] the Be(0001) surface,[22,23] TiO_2,[24] as well as high-temperature Fe-based superconductors.[25–27] The spectral function is characterized by a peak-dip-hump-like line shape and a two-branch behavior in the quasiparticle dispersion.[28] For further reading, we refer to Refs. 13 and 28–30.

Specifically for Fe, kinks were already found for surface[8] and bulk iron states.[9,11] The latter exhibit an energy renormalization at an energy of ∼270 meV in the majority-spin channel near the Fermi energy,[9] and even at a binding energy of 1.5 eV in the minority-spin bulk state,[11] while kinks in minority-surface resonances occur at an energy of ∼160 meV.[8] Based on the spin-wave energy scale of the kinks, they were attributed to dressing of electrons with magnons. The coupling constants of the low-energy band renormalizations were estimated as $\lambda = 0.14 \pm 0.03$[9] and 0.20 ± 0.04,[8] respectively. A successive study of a bulk band on Fe(110) reported on strong electron–electron interaction $\lambda \sim 1.7$ and weak phonon coupling $\lambda \sim 0.16$,[10] but a kink at 270 meV could not be confirmed.[9]

Comparing to manifestations of strong electron–phonon coupling, however, where besides kinks replica-band formation was

observed,[25,26] such kind of distinctive band renormalization has not been reported for electron–magnon coupling.

In the present study, we use spin- and angle-resolved laser photoelectron spectroscopy to unravel the coupling between fermionic quasiparticles and magnons. For a 15 monolayer (ML) iron film on W(110), we study not only the dispersion and spin polarization of a renormalized surface resonance but also the magnetic linear dichroism (MLD) in spin-polarized photoemission. We observe a pronounced two-branch splitting with a momentum-dependent transfer of spectral weight. MLD suggests the magnetic character of the band renormalization and, thereby, confirms the momentum-dependence of the electron–magnon coupling. One-step photoemission calculations based on relativistic band structure calculations reproduce the unperturbed surface-state band dispersion. By computing the quasiparticle dispersion due to different types of the electron–boson interaction, we show that the observed band renormalization is consistent with strong electron–magnon coupling of the surface state to an optical spin wave in the thin Fe film.

The 15-ML-thick Fe(110) samples were grown *in situ* on a W(110) substrate, that was cleaned beforehand by oxygen treatment. Iron was evaporated from a 2-mm rod (purity 99.995%) in an EFM3 evaporator (Focus). The deposition rate was 2 Å per minute. The first 2 ML was grown at 300 K. During deposition of the subsequent layers, the temperature was raised to 530 K at a rate of 1.5 K/s, where it was kept during the remaining evaporation and for 10 min additional annealing time. We used the various coverage-dependent superstructures observed in low-energy electron diffraction[31] in combination with a quartz microbalance to calibrate the evaporation rate and control the surface quality of the 15-ML-thick bcc Fe film. In addition, annealing temperature and surface quality were confirmed following the intensity of the $n = 1$ image-potential state in two-photon photoemission (2PPE). The Fe film is in-plane magnetized along the $[1\bar{1}0]$-direction [see Fig. 1(a), inset] with a Curie temperature close to bulk Fe.[32–34] All measurements have been performed at a sample temperature of 90 K.

In the spin-resolved photoemission experiment, we study the $\Sigma_{3,1}$ minority-spin surface resonance along the $\bar{\Gamma} - \bar{\mathrm{H}}$ direction of the Fe(110) surface Brillouin zone. We use linearly *p*-polarized light and a photon energy of 6.3 eV and bandwidth of 30 meV. Photoelectrons are detected after a cylindrical sector analyzer (CSA) by an exchange scattering spin detector.[35] The CSA and its lens system are optimized for high transmission of electrons with kinetic energy below 2 eV.[36] Thus, angular and energy resolution are moderate with ±2.5° and 65 meV, respectively. The former is defined by an aperture at the CSA entrance-lens, the latter was deduced from the low energy cutoff of the photoemission spectra. To determine the spin polarization of the photoemitted electrons, we can either revert the magnetization of the oxygen-passivated Fe/W(100) spin-filter crystal or of our Fe sample. Combining both, e.g., for the Gd surface-state,[12,37] we confirmed that spin polarization and MLD are not influenced by magnetic stray fields.

The inset in Fig. 1(a) illustrates the experimental geometry. At normal electron emission ($\vartheta = 0°$), the light was incident at an angle of 45°, at which the vector field **A** of the laser pulse contains equal parts of polarization parallel ($\boldsymbol{A}_{||}$) and perpendicular ($\boldsymbol{A}_{\perp}$) to the sample surface. Rotation of the sample to larger emission angles ϑ increases $\boldsymbol{A}_{||}$ and reduces $\boldsymbol{A}_{\perp}$. Since the magnetization, $\boldsymbol{M}||[1\bar{1}0]$, lies in the rotation axis of the sample, the spin quantization axis is unaffected when varying ϑ. According to the dipole selection rules, with a Σ_1-symmetric final state, electrons can be photoemitted from Σ_1 states by the $\boldsymbol{A}_{\perp}$ component and from Σ_3 states by the $\boldsymbol{A}_{||}$ component.[38] A series of 2PPE measurements confirming the $\Sigma_{3,1}$ spatial symmetry character of the observed surface resonance is presented in the supplementary material, Figs. S1 and S2.

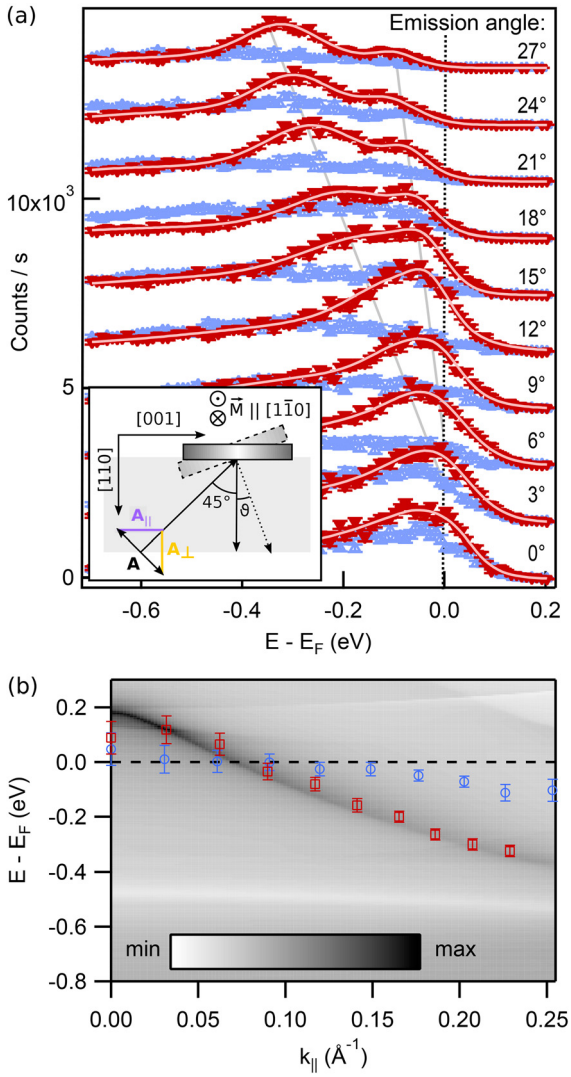

FIG. 1. Spin- and angle-resolved photoemission spectroscopy. (a) Energy distribution curves as a function of emission angle for minority- and majority-spin components (red tip-down and blue tip-up triangles). The light gray lines are guides to the eye along the dispersion of the minority-spin peaks. The inset represents the measurement geometry in a schematic view on the light-incidence plane (gray). (b) Minority-spin photoemission intensities computed in a one-step photoemission calculation (dark gray band) with the LSDA + DMFT approach. For comparison, the experimental peak positions are shown as red and blue symbols and have been extracted from fits to the minority-spin spectra in (a). In (b), $k_{||} = 0$ corresponds to normal emission ($\vartheta = 0°$) in (a). The data points for increasing parallel momentum in (b) correspond to increasing emission angles in (a).

The dispersion of the surface resonance along $\bar{\Gamma} - \bar{H}$ is shown in Fig. 1(a), in a series of spin-resolved spectra measured at different polar angles ϑ from 0° to 27° [$k_{||} \sim 0$ to 0.25 Å^{-1}, see data points in Fig. 1(b)]. We analyzed the spectra by a global fit including two Voigt profiles cut by the Fermi distribution. The position of the Fermi energy E_F was determined from the low-energy cutoff and the photon energy. Figure 1(b) summarizes the fitted peak positions, i.e., the dispersion of the two bands $E(k_{||})$ as a function of parallel momentum $k_{||}$. To analyze the origin of the minority-spin band splitting, we performed calculations based on the local spin-density approximation plus dynamical mean-field theory (LSDA + DMFT) approach [see the supplementary material, Figs. S1(c) and S3]. A one-step photoemission calculation of the minority-spin intensity for a photon energy of 6.3 eV is shown in Fig. 1(b), which agrees well with the measured main peak positions of the surface resonance (red squares). The surface resonance disperses downward in energy and thereby parallels the dispersion of the related $\Sigma_{3,1}$ bulk band. The strong minority-spin character of the surface resonance (see the supplementary material, Fig. S5) corroborates the spin-resolved photoemission and inverse photoemission results in Refs. 18 and 39, respectively. The one-step photoemission calculations in Ref. 39, furthermore, explain how the corresponding majority-spin surface resonance is shifted above the Fermi level E_F and is not detected in our experiment. We note that band structure calculations alone do usually not reveal the surface resonances, since bandgaps in the surface-projected bulk band structure of iron are much too small to be clearly separated surface from bulk bands (for the surface-projected bulk band structure along $\bar{\Gamma} - \bar{N}$ and $\bar{\Gamma} - \bar{H}$, see the supplementary material, Fig. S4). In fact we need to perform calculations within the one-step model of photoemission (1SM) to project-out surface resonances by the coupling to photocurrent carrying final states.[39,40] Compared to initial bulk states the coupling to free-electron-like final states is facilitated since surface resonances show no dispersion $E(k_\perp)$ as a function of perpendicular momentum $k_\perp$ and appear as peaks in 1SM calculations. Furthermore, the inelastic mean free path for iron is only about 3 ML even at low energies due to d-electron excitations.[41] For our present calculation, we use exactly the same LSDA + DMFT + 1SM approach and parameters as described in Refs. 18, 42, and the supplementary material, which includes correlations, matrix elements, and surface effects. The validity of this state-of-the-art approach may be seen from the experiment-theory comparison in Ref. 18. For further detailed discussion, we refer to Ref. 42.

In photoemission, the surface resonance appears at 0.08 Å^{-1} [$\sim$9° emission angle, Fig. 1(a)]. For emission angles >12° ($\sim$0.12 Å^{-1}), the minority-spin surface resonance clearly starts to split into two peaks, one with a steeper and one with a flatter dispersion meeting at E_F [indicated by the gray guidelines to the eye in Fig. 1(a)]. The theoretical photoemission spectra in Fig. 1(b), derived from the 1SM for a photon energy of 6.3 eV and based on the LSDA + DMFT calculated band structure and wave functions (see the supplementary material, Figs. S3 and S4), predict that there is only one single dispersing band and no second band to explain the flatter dispersing feature in the measured spectra (blue circles).

As we apply a fully relativistic band structure calculation, we rule out spin–orbit splitting of the surface resonance as the reason for our observation. Knowing that both states have either Σ_3 or Σ_1 spatial symmetry and are of minority-spin character, the corresponding bands should avoid a crossing and form a hybridization gap.[43] In other words, spin–orbit interaction leads to a lowering of already existing and crossing bands. Therefore, hybridization gaps open in the band structure, which for iron amount to $\leq$ 60 meV (see Fig. S3 and further discussion in the supplementary material).[44] Most important, spin–orbit coupling does not lead to a new, second split-off band and can, thus, not explain our experimental observation.

While the intensity of the second branch increases toward the Fermi level E_F, our energy and angular resolution are not sufficient to clearly resolve its spectral enhancement at E_F.[22,23] We conclude that both peaks must originate from the same surface resonance, i.e., the single undressed surface band as given by the LSDA + DMFT + 1SM calculations splits through quasiparticle renormalization into two dispersing branches.

Next, we discuss the occurrence of MLD appearing jointly with the energy renormalization. The measurement geometry in Fig. 1(a) fulfills the general requirement $|\boldsymbol{A} \cdot (\boldsymbol{M} \times \boldsymbol{k})| > 0$ for MLD in photoemission, which is similar to the transversal magneto-optical Kerr effect. Figure 2 shows pairs of minority-spin spectra with the sample magnetized in opposite directions, i.e., for spin magnetic moments aligned antiparallel to M+ and M−, respectively. These pairs of minority spin spectra have each been measured at a fixed angle in the $k_{||}$ range in which we find both peaks simultaneously. For M+, the renormalized state closer to E_F is seen as a shoulder to the main peak (Fig. 2). Upon reversal of the magnetization to M−, the intensity of the dressed state increases to form a peak-like structure, while the intensity of the main peak decreases slightly. A complete $E(k_{||})$-map of MLD in the minority-spin channel can be found in the supplementary material, Fig. S6(a).

Since MLD is a signature of coupling between spin and momentum space, the observed MLD is as well a consequence of the electron–magnon coupling. Regarding the spin system, spin-polarized electron energy loss spectroscopy (SPEELS)[45,46] gives already evidence for an asymmetric coupling of magnons to the electronic system. This shows up in different magnonic lifetimes for opposite wave vectors,[47] which have been assigned to the asymmetric Dzyaloshinskii–Moriya

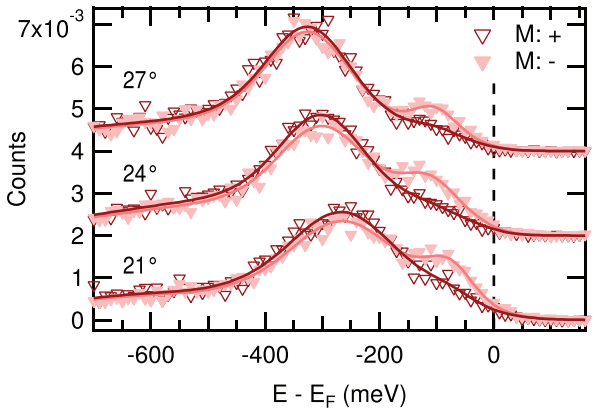

FIG. 2. Pairs of minority-spin spectra for reversed sample magnetization directions M+ and M−, measured at emission angles of 21°, 24°, and 27°. Total peak areas have been normalized for equal spectral weight. The reversal of the magnetization direction changes the spectral weight of both peaks leading to the MLD in the minority spin channel.

exchange interaction—just like the Rashba splitting observed in the magnon band structure.[45] Regarding the electronic system, this asymmetry will influence the magnon-induced renormalization in the photoemission spectrum, leads to the observed redistribution of the spectral weight between dressed and undressed states, and corroborates the magnetic nature of the electron dressing.

The LSDA + DMFT calculations account for the electron–electron interaction and LSDA + DMFT + 1SM give, thus, the bare minority-spin surface state, but do not take into account quasiparticle renormalization due to electron–phonon, magnon, or plasmon interactions. To analyze the effect of electron–boson renormalization, we start with considering a generic interaction Hamiltonian,

$$\mathcal{H} = \sum_{\boldsymbol{k}} \varepsilon_{\boldsymbol{k}} c^{\dagger}_{\boldsymbol{k}} c_{\boldsymbol{k}} + \sum_{\boldsymbol{q},\nu} \hbar\omega_{\boldsymbol{q}\nu} \left(b^{\dagger}_{\boldsymbol{q}\nu} b_{\boldsymbol{q}\nu} + \frac{1}{2} \right) + \sum_{\boldsymbol{q},\nu} \sum_{\boldsymbol{k}} I_{\nu} c^{\dagger}_{\boldsymbol{k}+\boldsymbol{q}} c_{\boldsymbol{k}} \left(b_{\boldsymbol{q}\nu} + b^{\dagger}_{-\boldsymbol{q}\nu} \right), \tag{1}$$

where the first (second) term describes the electron (boson) kinetic energy with band energy $\varepsilon_{\boldsymbol{k}}$ and boson energy $\hbar\omega_{\boldsymbol{q}\nu}$, respectively. The third term is the potential energy due to their mutual interaction with interaction strength I_{ν}. Using the Matsubara formalism on the imaginary axis and analytic continuation to the real frequency axis, the electron–boson interaction leads to the real-frequency-dependent electron self-energy at temperature T,[48,49]

$$\Sigma(\boldsymbol{k},\omega) = -T \sum_{n=-\infty}^{\infty} \sum_{\boldsymbol{k}',\nu} I_{\nu}^2 \left\{ D_{\nu}(\boldsymbol{q}, \omega - i\omega_n) G(\boldsymbol{k}', i\omega_n) - \sum_{\pm} \pm \frac{G_R(\boldsymbol{k}', \omega \pm \omega_{\boldsymbol{q}\nu})}{2} \left(\tanh \frac{\omega \pm \omega_{\boldsymbol{q}\nu}}{2T} \mp \coth \frac{\omega_{\boldsymbol{q}\nu}}{2T} \right) \right\}, \tag{2}$$

where

$$D_{\nu}(\boldsymbol{q}, i\omega_n - i\omega_{n'}) = \frac{-2\omega_{\boldsymbol{q}\nu}}{(\omega_n - \omega_{n'})^2 + \omega^2_{\boldsymbol{q}\nu}} \tag{3}$$

is the branch-resolved magnon Matsubara propagator for fermionic Matsubara frequencies, $\omega_n = (2n+1)\pi k_B T$. $G(\boldsymbol{k}, i\omega_n)$, $G_R(\boldsymbol{k}, \omega)$ are the Matsubara frequency dependent and retarded, real-frequency dependent full Green functions. The latter is given by

$$G_R^{-1}(\boldsymbol{k},\omega) = \left[G_0^R\right]^{-1}(\boldsymbol{k},\omega) - \Sigma(\boldsymbol{k},\omega),$$

with the bare Green function, $G_0^R(\boldsymbol{k},\omega) = [\omega + i\delta - \varepsilon_{\boldsymbol{k}}]^{-1}$, where δ is small and corresponds to physical broadening.

We solve Eq. (2) with a one-step calculation, employing the one-loop approximation:

$$G_R^{-1}(\Sigma) \approx G_0^{-1} - \Sigma(G_0), \tag{4}$$

which is reasonable since we are interested in qualitative features of the spectra due to poles of the electronic spectral function. Subsequently, from Eq. (4), we calculate the electron spectral function, $A(\boldsymbol{k},\omega) = -\pi^{-1}\mathrm{Im}\, G_R(\boldsymbol{k},\omega)$, which is proportional to the photoemission spectra. We approximate the bare electron dispersion in Fig. 1(b) as $\varepsilon_{\boldsymbol{k}} = t\cos(\boldsymbol{k}a_0) - \mu$, with $t = 200$ meV, $\mu = 300$ meV and consider next its coupling to specific magnon branches. The spin wave spectra of ultrathin Co and Fe films were extensively investigated in the past.[46,50–52] Due to the spatial confinement, thin Fe bcc(110) films exhibit acoustic as well as gapped optical spin wave branches that can be parametrized using Heisenberg exchange constants,

$$\omega_a(\boldsymbol{q}) = 12J_N \left[1 - \cos\left(\frac{\boldsymbol{q}a_0}{2} \right) \right] + 4J_{NN}[1 - \cos(\boldsymbol{q}a_0)], \tag{5}$$

$$\omega_o(\boldsymbol{q}) = 4J_N \left[3 - \cos\left(\frac{\boldsymbol{q}a_0}{2} \right) \right] + 4J_{NN}[3 - \cos(\boldsymbol{q}a_0)], \tag{6}$$

where $\boldsymbol{q} = \boldsymbol{q}_{\parallel}$, the in-plane momentum, $a_0 = 3.165$ Å is the lattice constant, and $J_N = 7.6$ meV and $J_{NN} = 4.6$ meV are the nearest and next-nearest neighbor exchange constants[50] (see the supplementary material, Fig. S7 for a sketch of the dispersion relations). Next, we compute the spectral function considering acoustic or optical magnons, or a dispersionless Einstein phonon mode with frequency $\Omega_0 = 40$ meV, while varying the interaction strength I_{ν} and using $\delta = 1.5$ meV. The spectral function computed for an optical magnon branch (see the supplementary material, Fig. S7), shown in Fig. 3, provides qualitative agreement with experiment. It shows a peak-dip-hump-like line shape with a dip at approximately 180 meV and a two-branch behavior in the quasiparticle dispersion. Due to the finite angular and energy resolution of our spin-resolved experiment, we cannot clearly resolve the transition from the bare dispersing quasiparticle to the dressed state in Fig. 1(a). Nevertheless, the spectral shape becomes at 0.12 Å^{-1} ($\vartheta = 12°$) asymmetric and evolves for increasing

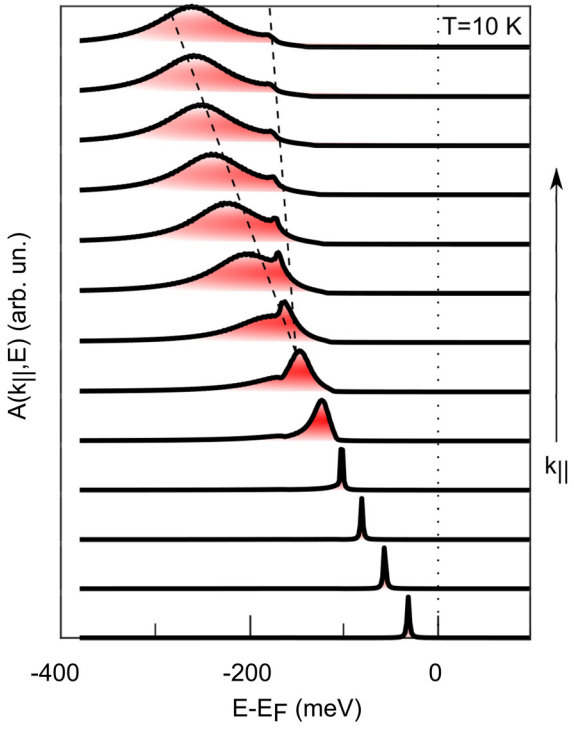

FIG. 3. Computed quasiparticle spectral density due to electron–magnon coupling to an optical magnon branch that has a characteristic frequency in the range 120–160 meV. The interaction strength I_o is here 110 meV.

parallel momentum (increasing ϑ) into a weakly dispersing peak at low-energy renormalized by electron–magnon coupling and a broader bare quasiparticle band at higher energy with stronger dispersion, separated by a dip at around 180 meV. Similar to the experiment, the spectral enhancement of the low-energy peak is very moderate in our calculation. This scenario corresponds for example to the coupling of the H-induced surface state on W(110) to the adsorbate's stretch-vibration[14] while the transfer of spectral weight is much stronger for the Be(0001) surface state dressed by acoustic phonons.[22] Further illustrations for band renormalization due to the acoustic magnon and Einstein phonon modes are given in the supplementary material, Fig. S8. As observed for H/W(110) renormalization due to an Einstein phonon mode can also lead to branch splitting. However, since the largest phonon frequency in bcc Fe is 40 meV,[53] the split-off quasiparticle branch stays close to the Fermi energy, see the supplementary material, Fig. S8(a).

The interaction with the optical magnon mode, conversely, causes an unusual, strongly momentum-dependent renormalization of the surface state. While in the past, a kink has been detected,[8] here we find a splitting of the bare electron dispersion in two quasiparticle bands. Specifically, the spectral density at lower binding energy is a momentum-dependent replica of the state at higher binding energy, a feature that has not been reported before for electron–magnon coupling. It is similar to the appearance of replica-band formation[24–27] due to the electron–phonon interaction,[54,55] where, however, it is practically momentum independent.

Previously, the bulk electron–magnon coupling constant λ of Fe was estimated from the self-energy $\Sigma(\boldsymbol{k}, \omega)$ measured by angle-resolved photoemisson spectroscopy (ARPES), giving $\lambda \sim 0.14$.[9] For the surface resonance ($\lambda \sim 0.2$), it was estimated from the kink in the band dispersion.[8] However, this procedure is less accurate and cannot be employed in our case. We directly compute the coupling constant λ_ν by the general formula

$$\lambda_\nu = N_0 \left\langle \left\langle \frac{2I_\nu^2}{\omega_{\boldsymbol{q}\nu}} \right\rangle_{\boldsymbol{k}_F'} \right\rangle_{\boldsymbol{k}_F} \tag{7}$$

with $N_0 = 0.0012$ states/meV the density of states at the Fermi level of the electron band and $\langle \cdots \rangle_{\boldsymbol{k}_F}$ a momentum average over the Fermi surface. This procedure yields $\lambda_o = 0.2$ for the optical magnon. Although at the first sight this value does not seem large compared to strong electron–phonon coupling constants $\lambda \sim 1$, it deserves to be noted that the magnon frequency in the denominator of Eq. (7) is much larger than typical phonon frequencies. Recalculating the coupling constant for a 40 meV-phonon frequency gives that it would correspond to an electron–phonon coupling with $\lambda = 0.7$, thus indicating a comparably strong coupling. Finally, as was shown previously, these spin waves are strongly damped.[56,57] The robust coupling of electrons to these optical magnons could provide a relevant channel for ultrafast laser-induced demagnetization[6,37,58] in thin films that has so far not been considered.

In summary, we find a remarkable quasiparticle renormalization of the minority-spin surface resonance on Fe(110). The renormalization occurs in the typical energy range (160–200 meV) for magnonic excitations in thin Fe/W(110) films,[59] and its magnetic nature is further corroborated by a redistribution in the MLD spectral weight upon reversal of the sample magnetization. Our findings particularly reveal that in an elementary ferromagnet, electronic states can show exceptional coupling to spin excitations. This adds knowledge regarding the coupling to magnons and spin fluctuations and contributes to obtaining a better understanding of ultrafast spin dynamics in thin magnetic systems.

See the supplementary material; we present data on the sample preparation, spectroscopic analysis (1SM), symmetry and spin character of the surface resonance, surface-projected bulk band structure, and information on the LSDA + DMFT and quasiparticle spectrum calculations.

B.A., M.W., and P.M.O. acknowledge funding by the Deutsche Forschungsgemeinschaft through CRC/TRR 227 "Ultrafast spin Dynamics," projects A01 and MF. J.B. and H.E. acknowledge support from the Deutsche Forschungsgemeinschaft (Grant Nos. EB 154/32 and EB 154/37), and the Bundesministerium für Bildung und Forschung through No. BMBF: 05K16WMA for financial support. A.A. and P.M.O. acknowledge support from the Swedish Research Council (VR), the K & A Wallenberg Foundation (Grant No. 2015.0060), the Röntgen-Ångström Cluster, and the Swedish National Infrastructure for Computing (SNIC). The authors would like to thank Focus GmbH for their steady support of the CSA analyzer over two decades.

AUTHOR DECLARATIONS

Conflict of Interest

The authors have no conflicts to disclose.

Author Contributions

B.A. and M.W. designed the experiment. B.A. performed the experiment. J.B. and H.E. performed the *ab initio* calculations of photoelectron spectra. A.A. and P.M.O. simulated the quasiparticle spectra. B.A., M.W., and P.M.O. wrote the paper with input from all coauthors.

DATA AVAILABILITY

The data that support the findings of this study are available within the article and its supplementary material.

REFERENCES

[1] T. Balashov, A. F. Takács, M. Däne, A. Ernst, P. Bruno, and W. Wulfhekel, Phys. Rev. B **78**, 174404 (2008).
[2] M. Haag, C. Illg, and M. Fähnle, Phys. Rev. B **90**, 014417 (2014).
[3] E. Carpene, H. Hedayat, F. Boschini, and C. Dallera, Phys. Rev. B **91**, 174414 (2015).
[4] E. Turgut, D. Zusin, D. Legut, K. Carva, R. Knut, J. M. Shaw, C. Chen, Z. Tao, H. T. Nembach, T. J. Silva, S. Mathias, M. Aeschlimann, P. M. Oppeneer, H. C. Kapteyn, M. M. Murnane, and P. Grychtol, Phys. Rev. B **94**, 220408 (2016).
[5] S. Eich, M. Plötzing, M. Rollinger, S. Emmerich, R. Adam, C. Chen, H. C. Kapteyn, M. M. Murnane, L. Plucinski, D. Steil, B. Stadtmüller, M. Cinchetti, M. Aeschlimann, C. M. Schneider, and S. Mathias, Sci. Adv. **3**, e1602094 (2017).
[6] P. Tengdin, W. You, C. Chen, X. Shi, D. Zusin, Y. Zhang, C. Gentry, A. Blonsky, M. Keller, P. M. Oppeneer, H. C. Kapteyn, Z. Tao, and M. M. Murnane, Sci. Adv. **4**, eaap9744 (2018).
[7] R. Gort, K. Bühlmann, S. Däster, G. Salvatella, N. Hartmann, Y. Zemp, S. Holenstein, C. Stieger, A. Fognini, T. U. Michlmayr, T. Bähler, A. Vaterlaus, and Y. Acremann, Phys. Rev. Lett. **121**, 087206 (2018).

[8]J. Schäfer, D. Schrupp, E. Rotenberg, K. Rossnagel, H. Koh, P. Blaha, and R. Claessen, Phys. Rev. Lett. **92**, 097205 (2004).
[9]X. Y. Cui, K. Shimada, M. Hoesch, Y. Sakisaka, H. Kato, Y. Aiura, M. Higashiguchi, Y. Miura, H. Namatame, and M. Taniguchi, Surf. Sci. **601**, 4010 (2007).
[10]X. Y. Cui, K. Shimada, Y. Sakisaka, H. Kato, M. Hoesch, T. Oguchi, Y. Aiura, H. Namatame, and M. Taniguchi, Phys. Rev. B **82**, 195132 (2010).
[11]E. Mlyńczak, M. C. T. D. Müller, P. Gospodaric, T. Heider, I. Aguilera, G. Bihlmayer, M. Gehlmann, M. Jugovac, G. Zamborlini, C. Tusche, S. Suga, V. Feyer, L. Plucinski, C. Friedrich, S. Blügel, and C. M. Schneider, Nat. Commun. **10**, 505 (2019).
[12]B. Liu, H. Xiao, G. Siemann, J. Weber, B. Andres, W. Bronsch, P. M. Oppeneer, and M. Weinelt, Phys. Rev. B **104**, 024434 (2021).
[13]*Angle-Resolved Photoemission*, edited by S. D. Kevan (Elsevier, Amsterdam, 1992).
[14]E. Rotenberg, J. Schäfer, and S. D. Kevan, Phys. Rev. Lett. **84**, 2925 (2000).
[15]A. Lanzara, P. V. Bogdanov, X. J. Zhou, S. A. Kellar, D. L. Feng, E. D. Lu, T. Yoshida, H. Eisaki, A. Fujimori, K. Kishio, J.-I. Shimoyama, T. Noda, S. Uchida, Z. Hussain, and Z.-X. Shen, Nature **412**, 510 (2001).
[16]P. Hofmann, E. V. Chulkov, and I. Y. Sklyadneva, "Electron-phonon interaction at interfaces," in *Dynamics at Solid State Surfaces and Interfaces: Volume 1: Current Developments* (Wiley-VCH Verlag, 2010), pp. 145–165.
[17]K. Byczuk, M. Kollar, K. Held, Y.-F. Yang, I. A. Nekrasov, T. Pruschke, and D. Vollhardt, Nat. Phys. **3**, 168 (2007).
[18]J. Sánchez-Barriga, J. Fink, V. Boni, I. D. Marco, J. Braun, J. Minár, A. Varykhalov, O. Rader, V. Bellini, F. Manghi, H. Ebert, M. I. Katsnelson, A. I. Lichtenstein, O. Eriksson, W. Eberhardt, and H. A. Dürr, Phys. Rev. Lett. **103**, 267203 (2009).
[19]J. Schäfer, M. Hoinkis, E. Rotenberg, P. Blaha, and R. Claessen, Phys. Rev. B **72**, 155115 (2005).
[20]G. G. Lonzarich, J. Magn. Magn. Mater. **45**, 43 (1984).
[21]A. Bostwick, T. Ohta, T. Seyller, K. Horn, and E. Rotenberg, Nat. Phys. **3**, 36 (2007).
[22]M. Hengsberger, D. Purdie, P. Segovia, M. Garnier, and Y. Baer, Phys. Rev. Lett. **83**, 592 (1999).
[23]S. LaShell, E. Jensen, and T. Balasubramanian, Phys. Rev. B **61**, 2371 (2000).
[24]S. Moser, L. Moreschini, J. Jaćimović, O. S. Barišić, H. Berger, A. Magrez, Y. J. Chang, K. S. Kim, A. Bostwick, E. Rotenberg, L. Forró, and M. Grioni, Phys. Rev. Lett. **110**, 196403 (2013).
[25]J. J. Lee, F. T. Schmitt, R. G. Moore, S. Johnston, Y.-T. Cui, W. Li, M. Yi, Z. K. Liu, M. Hashimoto, Y. Zhang, D. H. Lu, T. P. Devereaux, D.-H. Lee, and Z.-X. Shen, Nature **515**, 245 (2014).
[26]S. N. Rebec, T. Jia, C. Zhang, M. Hashimoto, D.-H. Lu, R. G. Moore, and Z.-X. Shen, Phys. Rev. Lett. **118**, 067002 (2017).
[27]S. Choi, S. Johnston, W.-J. Jang, K. Koepernik, K. Nakatsukasa, J. M. Ok, H.-J. Lee, H. W. Choi, A. T. Lee, A. Akbari, Y. K. Semertzidis, Y. Bang, J. S. Kim, and J. Lee, Phys. Rev. Lett. **119**, 107003 (2017).
[28]A. Damascelli, Z. Hussain, and Z.-X. Shen, Rev. Mod. Phys. **75**, 473 (2003).
[29]E. V. Chulkov, K. Ishioka, S. W. Koch, J. M. Pitarke, J. Schäfer, and M. Weinelt, "Quasiparticles and collective excitations," in *Dynamics at Solid State Surfaces and Interfaces: Volume 2-Fundamentals* (Wiley-VCH Verlag, 2010), pp. 27–106.
[30]J. A. Sobota, Y. He, and Z.-X. Shen, Rev. Mod. Phys. **93**, 025006 (2021).
[31]U. Gradmann and G. Waller, Surf. Sci. **116**, 539 (1982).
[32]U. Gradmann, J. Korecki, and G. Waller, Appl. Phys. A **39**, 101 (1986).
[33]M. Stampanoni, A. Vaterlaus, M. Aeschlimann, and F. Meier, Phys. Rev. Lett. **59**, 2483 (1987).
[34]S. Miesch, A. Fognini, Y. Acremann, A. Vaterlaus, and T. U. Michlmayr, J. Appl. Phys. **109**, 013905 (2011).
[35]A. Winkelmann, D. Hartung, H. Engelhard, C.-T. Chiang, and J. Kirschner, Rev. Sci. Instrum. **79**, 083303 (2008).
[36]M. Weinelt, A. B. Schmidt, M. Pickel, and M. Donath, Prog. Surf. Sci. **82**, 388 (2007).
[37]B. Andres, M. Christ, C. Gahl, M. Wietstruk, M. Weinelt, and J. Kirschner, Phys. Rev. Lett. **115**, 207404 (2015).
[38]J. Hermanson, Solid State Commun. **22**, 9 (1977).
[39]J. Braun, C. Math, A. Postnikov, and M. Donath, Phys. Rev. B **65**, 184412 (2002).
[40]T. Allmers, M. Donath, J. Braun, J. Minár, and H. Ebert, Phys. Rev. B **84**, 245426 (2011).
[41]D. P. Pappas, K.-P. Kämper, B. P. Miller, H. Hopster, D. E. Fowler, C. R. Brundle, A. C. Luntz, and Z.-X. Shen, Phys. Rev. Lett. **66**, 504 (1991).
[42]J. Sánchez-Barriga, J. Braun, J. Minár, I. D. Marco, A. Varykhalov, O. Rader, V. Boni, V. Bellini, F. Manghi, H. Ebert, M. I. Katsnelson, A. I. Lichtenstein, O. Eriksson, W. Eberhardt, H. A. Dürr, and J. Fink, Phys. Rev. B **85**, 205109 (2012).
[43]A. Rampe, G. Güntherodt, D. Hartmann, J. Henk, T. Scheunemann, and R. Feder, Phys. Rev. B **57**, 14370 (1998).
[44]M. Pickel, A. B. Schmidt, F. Giesen, J. Braun, J. Minár, H. Ebert, M. Donath, and M. Weinelt, Phys. Rev. Lett. **101**, 066402 (2008).
[45]K. Zakeri, Y. Zhang, J. Prokop, T.-H. Chuang, N. Sakr, W. X. Tang, and J. Kirschner, Phys. Rev. Lett. **104**, 137203 (2010).
[46]K. Zakeri, Phys. Rep. **545**, 47 (2014).
[47]K. Zakeri, Y. Zhang, T. H. Chuang, and J. Kirschner, Phys. Rev. Lett. **108**, 197205 (2012).
[48]F. Marsiglio, M. Schossmann, and J. P. Carbotte, Phys. Rev. B **37**, 4965 (1988).
[49]F. Marsiglio, Phys. Rev. B **42**, 2416 (1990).
[50]Y. Zhang, "High wave vector spin waves in ultrathin Fe films on W(110) studied by spin-polarized electron energy loss spectroscopy," Ph.D. thesis (Martin-Luther University, Halle-Wittenberg, 2009).
[51]K. Zakeri, Y. Zhang, and J. Kirschner, J. Electron Spectrosc. Relat. Phenom. **189**, 157 (2013).
[52]Y.-J. Chen, K. Zakeri, A. Ernst, H. J. Qin, Y. Meng, and J. Kirschner, Phys. Rev. Lett. **119**, 267201 (2017).
[53]K. Carva, M. Battiato, D. Legut, and P. M. Oppeneer, Phys. Rev. B **87**, 184425 (2013).
[54]A. Aperis and P. M. Oppeneer, Phys. Rev. B **97**, 060501 (2018).
[55]F. Schrodi, A. Aperis, and P. M. Oppeneer, Phys. Rev. B **98**, 094509 (2018).
[56]A. T. Costa, R. B. Muniz, and D. L. Mills, Phys. Rev. B **68**, 224435 (2003).
[57]Y. Zhang, T.-H. Chuang, K. Zakeri, and J. Kirschner, Phys. Rev. Lett. **109**, 087203 (2012).
[58]E. Beaurepaire, J.-C. Merle, A. Daunois, and J.-Y. Bigot, Phys. Rev. Lett. **76**, 4250 (1996).
[59]T.-H. Chuang, K. Zakeri, A. Ernst, L. M. Sandratskii, P. Buczek, Y. Zhang, H. J. Qin, W. Adeagbo, W. Hergert, and J. Kirschner, Phys. Rev. Lett. **109**, 207201 (2012).